ARMY RESEARCH LABORATORY

Urban Turbulence Velocity Spectra From JU2003 Observation

by Sam Chang, Ananth Sridhar, Cheryl Klipp, and Giap Huynh

ARL-TR-7157 December 2014

NOTICES

Disclaimers

The findings in this report are not to be construed as an official Department of the Army position unless so designated by other authorized documents.

Citation of manufacturer's or trade names does not constitute an official endorsement or approval of the use thereof.

Destroy this report when it is no longer needed. Do not return it to the originator.

Army Research Laboratory
Adelphi, MD 20783-1138

ARL-TR-7157 **December 2014**

Urban Turbulence Velocity Spectra From JU2003 Observation

Sam Chang, Cheryl Klipp, and Giap Huynh
Computational and Information Sciences Directorate, ARL

Ananth Sridhar
Thomas Jefferson High School for Science and Technology
Alexandria, VA

REPORT DOCUMENTATION PAGE

Form Approved
OMB No. 0704-0188

1. REPORT DATE *(DD-MM-YYYY)*	2. REPORT TYPE	3. DATES COVERED (From - To)
December 2014		

4. TITLE AND SUBTITLE
Urban Turbulence Velocity Spectra From JU2003 Observation

5a. CONTRACT NUMBER

5b. GRANT NUMBER

5c. PROGRAM ELEMENT NUMBER

6. AUTHOR(S)
Sam Chang, Ananth Sridhar, Cheryl Klipp, and Giap Huynh

5d. PROJECT NUMBER

5e. TASK NUMBER

5f. WORK UNIT NUMBER

7. PERFORMING ORGANIZATION NAME(S) AND ADDRESS(ES)
U.S. Army Research Laboratory
ATTN: RDRL-CIE-D
2800 Powder Mill Road
Adelphi, MD 20783-1138

8. PERFORMING ORGANIZATION REPORT NUMBER
ARL-TR-7157

9. SPONSORING/MONITORING AGENCY NAME(S) AND ADDRESS(ES)

10. SPONSOR/MONITOR'S ACRONYM(S)

11. SPONSOR/MONITOR'S REPORT NUMBER(S)

12. DISTRIBUTION/AVAILABILITY STATEMENT
Approved for public release; distribution unlimited.

13. SUPPLEMENTARY NOTES

14. ABSTRACT
A simple analytical form is used to model turbulent velocity spectra. This form has 2 free constants that can be calculated by turbulence measurements with a non-linear curve fitting method. The Joint Urban 2003 (JU2003) field experiments were undertaken in Oklahoma City during the summer of 2003. Sonic anemometer data taken using Lawrence Livermore National Laboratory's 83 m pseudo tower from JU2003 are analyzed. We present the results of characteristics of the urban turbulence velocity spectra. In particular, we focus on the features of spectral peak frequency and wavelength. Their variations with wind direction and atmospheric stability, within and above the urban canopy, are discussed in detail.

15. SUBJECT TERMS
JU2003, Atmospheric Turbulence

16. SECURITY CLASSIFICATION OF:			17. LIMITATION OF ABSTRACT	18. NUMBER OF PAGES	19a. NAME OF RESPONSIBLE PERSON
a. REPORT	b. ABSTRACT	c. THIS PAGE			Sam Chang
Unclassified	Unclassified	Unclassified	UU	34	19b. TELEPHONE NUMBER (*Include area code*) (301) 394-1988

Standard Form 298 (Rev. 8/98)
Prescribed by ANSI Std. Z39.18

Contents

List of Figures

List of Tables

Acknowledgments

We thank Dr Julie Lundquist at LLNL for much help, and Dr Adam Wolf with the Department of Ecology and Evolutionary Biology, Princeton University, for his code to calculate co-spectra. We also thank Drs John Noble, Steve Hill, Dennis Garvey, and David Tofsted, and Mr Chatt Williamson at the US Army Research Laboratory (ARL) for having provided help and useful discussion. Mr Dennis Li, a 2009 ARL summer student from Langley High School, had contributed to the development of ARL spectral analyses codes.

1. Introduction

Spectral analyses of turbulent velocity fluctuations in the atmospheric boundary layer over flat terrains have been well studied (Busch and Panofsky, 1968; Panofsky and Dutton, 1984; Kaimal and Finnigan, 1994). However, they are poorly understood over urban areas due to the lack of sufficiently complete measurements of high quality and successful theoretical hypothesis (Feigenwinter, 1999, Roth, 2000). A major field experiment, the Joint Urban 2003 (JU2003) experiment, was a cooperative undertaking to study transport and dispersion in the atmospheric boundary layer in an urban environment. JU2003 was conducted in Oklahoma City in the summer of 2003 (Alwine et al., 2004). The Lawrence Livermore National Laboratory (LLNL) deployed a pseudo-tower of 83 m height at a downtown site, equipped with sonic anemometers at 8 levels (Lundquist, et al., 2004; Gouveia, et al., 2007). A large amount of sonic anemometer data from the LLNL pseudo-tower were collected, processed, and archived. We have computed and analyzed the turbulence velocity spectra from this data set and present the following results.

Turbulence velocity spectra and co-spectra can provide valuable insights into urban boundary layer structure. There are 2 important aspects that are still unclear and controversial. The first aspect is related to the peak frequency and peak wavelength within and above the urban canopy layer. The second is related to the local isotropy or the transition from anisotropic to isotropic turbulence in the urban boundary layer. This report presents the results for the first aspect. Results related to the second aspect will be presented in a separate paper.

The spectral peak frequency and the peak wavelength are of greater importance to boundary layer meteorologists than the integral length scale since they are representative of the size of the eddies with the most energy, as noted by Kaimal and Finnigan (1994). Previous studies on the spectral peaks for urban canopy flows were interested in 3 issues—the influences of the displacement height (d), the atmospheric stability, and the observation height on those spectral peaks. The results of those previous studies reviewed by Roth (2000) are controversial and uncertain. For example, the composite Fig. 11 in Roth's paper seems uncertain whether the non-dimensional spectral peak frequencies for the 3 wind components (u, v, and w) increase with increasing height for neutral conditions, although Feigenwinter et al. (1997, 1999) indicated a general increase of non-dimensional peak frequencies with increasing normalized height. On the other hand, the composite Fig. 12 in the same paper appears unclear whether the peak wavelengths for the 3 wind components decrease with increasing stability. Feigenwinter et al. (1999) have shown that the peak frequencies for u, v, and w spectra increase with height, but no clear relation of those peaks with atmospheric stability. Chang et al. (2004, 2009, 2010) have reported some new results on the spectral peaks from the JU2003 data. However, they have used only limited data of a few days from that data bank. Our current study presents new results on these 3 issues from the much larger and extensive JU2003 data set.

2. Model

Various analytical expressions have been reviewed and suggested to model turbulent velocity spectra and co-spectra for atmospheric boundary layer (Wilson, 1998, Lee et al. 2004). We use a simple form to model the one-dimensional turbulent velocity (*u, v, w*) spectra, as suggested by Sorbjan (1989), and Kaimal and Finnigan (1994):

$$Y = fS_i = \frac{a_i n}{(1+b_i n)^{\frac{5}{3}}}, \ldots i = u, v, w \quad (1)$$

where S_i is the power spectrum ($m^2 s^{-1}$) for the 3 wind components $i = u$, v, and w, f is the frequency (Hz), $n = \frac{fz}{\bar{u}}$ is the normalized (non-dimensional) frequency, z is the measurement height (m), and $\bar{u}$ is the mean wind speed at z. a_i and b_i are empirical constants. These empirical constants can absorb or connote some micrometeorological parameters such as u_* (friction velocity) and L (Obukhov length), where

$$u_* = ((\overline{u'w'})^2 + (\overline{v'w'})^2)^{\frac{1}{4}} \quad (2)$$

and

$$L = -\frac{u_*^3 T}{kg\overline{w'T'}} \quad (3)$$

where T is the Kelvin temperature, g is the acceleration due to gravity, and k is the Von Karman constant (0.40). The over-bars in these equations denote mean values—half-hour mean values in our data processing. Primes (u′, v′, w′, and T′) denote the deviations from their mean values, respectively.

Given the measured power spectrum from FFT, the experimental constants in Eq. 1 can be evaluated by the standard least square error method. Once the experimental constants (a_i and b_i) are determined, the spectral shape and the related spectral peak values can also be calculated as

$$N_i = \frac{3}{2b_i}, i = u, v, w \quad (4)$$

$$\Lambda_i = \frac{z}{N_i}, i = u, v, w \quad (5)$$

where N_i is the normalized peak frequency and Λ_i is the peak wavelength (m).

3. Data Analysis

Detailed information about the pseudo tower and sonic anemometer data has been provided by Lundquist et al., (2004) and Gouveia et al., (2007). The 83.2 m pseudo tower was a large crane-based system that provided a stable platform for sonic anemometers. Its location was 35° 28.55' N and 97° 31.07' W, just north of the central business district of Oklahoma City. The urban canopy of Oklahoma City is highly inhomogeneous. Figure 1 illustrates the building height situation around the tower. Lundquist et al. (2004) have shown the variation of building heights in the fetch upstream of the tower. Although the mean building height varies only slightly, 5–15 m, the maximum height varies considerably. For example, the variation of building height with distance from the tower for the 30° (165–195° in meteorological coordinates) arc south of the tower is dramatic, with mean height 12.8 m and one tall building height 113.5 m, as shown by Fig. 1.

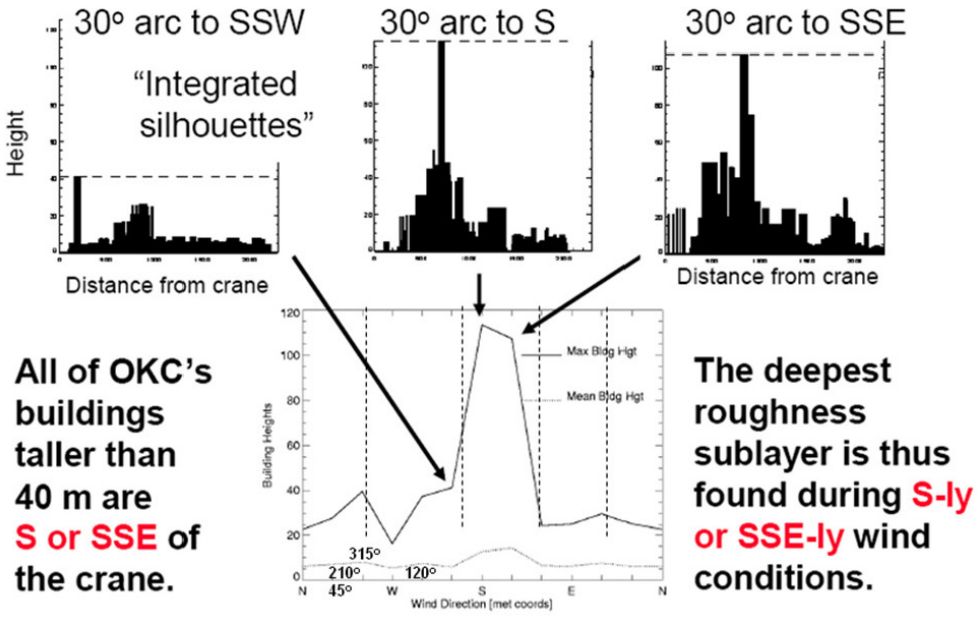

Fig. 1 Building height situation around the LLNL pseudo tower. The upper part shows the variation of building height with distance from the tower for the three 30° arcs: 135–165° (right), 165–195° (middle), and 195–225° (left), respectively. The lower part shows the variation of building height in the fetch upstream of the tower, presented as function of wind direction. The solid line indicates the maximum building height. The dotted line indicates the mean building height. Courtesy of Lundquist, Shinn and Gouveia (2004).

With the consideration of the building height variation with respect to wind direction (WD), we group the sonic data into 4 WD sectors:

1. 45° < WD < °120°

2. $120° < WD < 210°$
3. $210° < WD < 315°$
4. $315° < WD < 45°$

As suggested by Lundquist et al. (2004), the time periods during which the mean wind direction ranged between 315° and 45° were not used due to the pseudo tower's 'shadow effect'. The mean building heights in the 3 WD sectors 1, 2, and 3 are estimated as 6.6 m, 11.2 m, and 6.8 m, respectively.

Sonic anemometers were mounted on the pseudo-tower at heights of 7.8(A), 14.6(B), 21.5(C), 28.3(D), 42.5(E), 55.8(F), 69.7(G), and 83.2(H) m above ground level (AGL). The sonic anemometers (R.M. Young model 81000) measured 3 wind components and temperature at a sampling rate of 10 Hz for 35 days of measurements (from June 28 to August 1, Julian Day 179 to 213, 2003). The data set has been quality controlled and archived, and is open for public access. For this analysis, 31 days of data (July 1 to July 31) were used. Chang and Huynh (2007) have used several methods to estimate the roughness height (z_0) and the displacement height (d) for the 3 WD sectors. Their values for the 3 WD sectors are approximately

1. $z_0 = 0.93$ m, $d = 11.22$ m
2. $z_0 = 4.04$ m, $d = 19.93$ m
3. $z_0 = 0.66$ m, $d = 14.65$ m

For each day (24 h) of analysis, data was divided into 48 half-hour segments. This defines a "run" for turbulence analysis. Considering 48 blocks per day over the analysis period yields 1488 runs. However, some questionable data has been excluded. We exclude the data with extremely high or extremely small stability parameter values. The total number of runs is 1061, 1100, 1157, 1143, 1161, 1152, 1146, and 1180 for levels A through H, respectively. Table 1 provides data situation at 8 levels with respect to the 3 wind direction sectors used for present analyses.

Table 1 shows the following features for the data used in our analyses. First, the mean values of ζ (=z/L) are negative at every level. This indicates that the tower layer was unstable most times in July 2003. Second, the total number of runs for each of the 3 WD sectors at any of the 8 levels exceeds 1000, providing a large sample set for statistics shown in the next section. Finally, more than 70% of the data is in WD sector 2. This is primarily due to the prevailing wind direction for Oklahoma City in July 2003.

Table 1 Data situation at 8 levels with respect to the three wind direction (WD) sectors used for present analyses. Number of runs, $z/L(\zeta)$ range, its mean values, and standard deviations (σ) are listed for each level.

WD Sector		1	2	3	WD Sector		1	2	3
Level A 7.8 m	Run No.	96	851	114	Level B 14.6 m	Run No.	116	832	152
	Min ζ	–1.39	–2.33	–5.32		Min ζ	–1.85	–5.74	–2.16
	Max ζ	0.03	0.17	0.15		Max ζ	0.03	0.17	0.23
	Mean ζ	–0.135	–0.086	–0.217		Mean ζ	–0.166	–0.091	–0.213
	σ of ζ	0.19	0.132	0.599		σ of ζ	0.258	0.254	0.396
Level C 21.5 m	Run No.	135	816	206	Level D 28.3 m	Run No.	116	842	185
	Min ζ	–2.61	–2.40	–3.53		Min ζ	–3.21	–9.52	–3.76
	Max ζ	0.11	0.42	0.31		Max ζ	0.16	0.62	0.37
	Mean ζ	–0.189	–0.096	–0.226		Mean ζ	–0.213	–0.112	–0.275
	σ of ζ	0.311	0.172	0.430		σ of ζ	0.368	0.363	0.553
Level E 42.5 m	Run No.	128	871	162	Level F 55.8 m	Run No.	126	835	191
	Min ζ	–6.60	–5.27	–9.22		Min ζ	–6.56	–9.15	–5.90
	Max ζ	0.94	0.48	1.99		Max ζ	1.09	1.01	1.98
	Mean ζ	–0.430	–0.129	–0.375		Mean ζ	–0.449	–0.117	–0.346
	σ of ζ	0.951	0.333	1.089		σ of ζ	1.043	0.388	1.011
Level G 69.7 m	Run No.	120	859	167	Level H 83.2 m	Run No.	124	862	194
	Min ζ	–5.24	–5.15	–9.80		Min ζ	–8.28	–6.58	–8.30
	Max ζ	3.56	1.96	3.76		Max ζ	5.72	2.69	4.30
	Mean ζ	–0.273	–0.115	–0.386		Mean ζ	–0.191	–0.111	–0.415
	σ of ζ	1.182	0.376	1.482		σ of ζ	1.820	0.573	1.607

Sonic anemometer tilt correction was employed with a 2-angle rotation method (Kaimal and Finnigan, 1994). Computations for tilt correction ran on a block-by-block basis, yielding *u* (streamwise), *v* (transverse), and *w* (vertical) wind components. Turbulent components *u'*, *v'*, and *w'* were defined by deviation from a block's mean (Stull, 1988). Turbulence statistics for each block were calculated and used for other analyses.

FFT algorithms used in spectral analysis require input sizes of 2^n data points. We use 2^{14} (16384) data points—i.e., 1638.4 s (27'18.4")—of data from each half-hour run (18000 points). The FFT yields 2^{13} = 8192 output data points for each run. Given the $fS_i(j)$ for $j = 1 \ldots 2^{13}$ from FFT, the squared error is expressed as

$$\delta^2 = \sum \left(\left(Y_j\right)_{FFT} - \left(Y_j\right)_{model} \right)^2 \quad , \quad \text{j=1,2, } \ldots\ldots\ldots\ldots 2^{13} \tag{6}$$

The least squares method is used to determine the 2 parameters a_i and b_i in Eq. 1 by solving

$$\frac{\partial(\delta^2)}{\partial a_i} = 0 \tag{7}$$

and

$$\frac{\partial(\delta^2)}{\partial b_i} = 0. \tag{8}$$

Spectral values N_i and Λ_i can be easily calculated with Eqs. 4 and 5.

Figure 2 shows results obtained from the least-squares method to determine equations for the u, v, and w spectra. It should be noted that 46 bin averaged points were used instead of the 8192 points from the FFT. This is done to produce a smooth curve in the presence of large fluctuations in high frequencies.

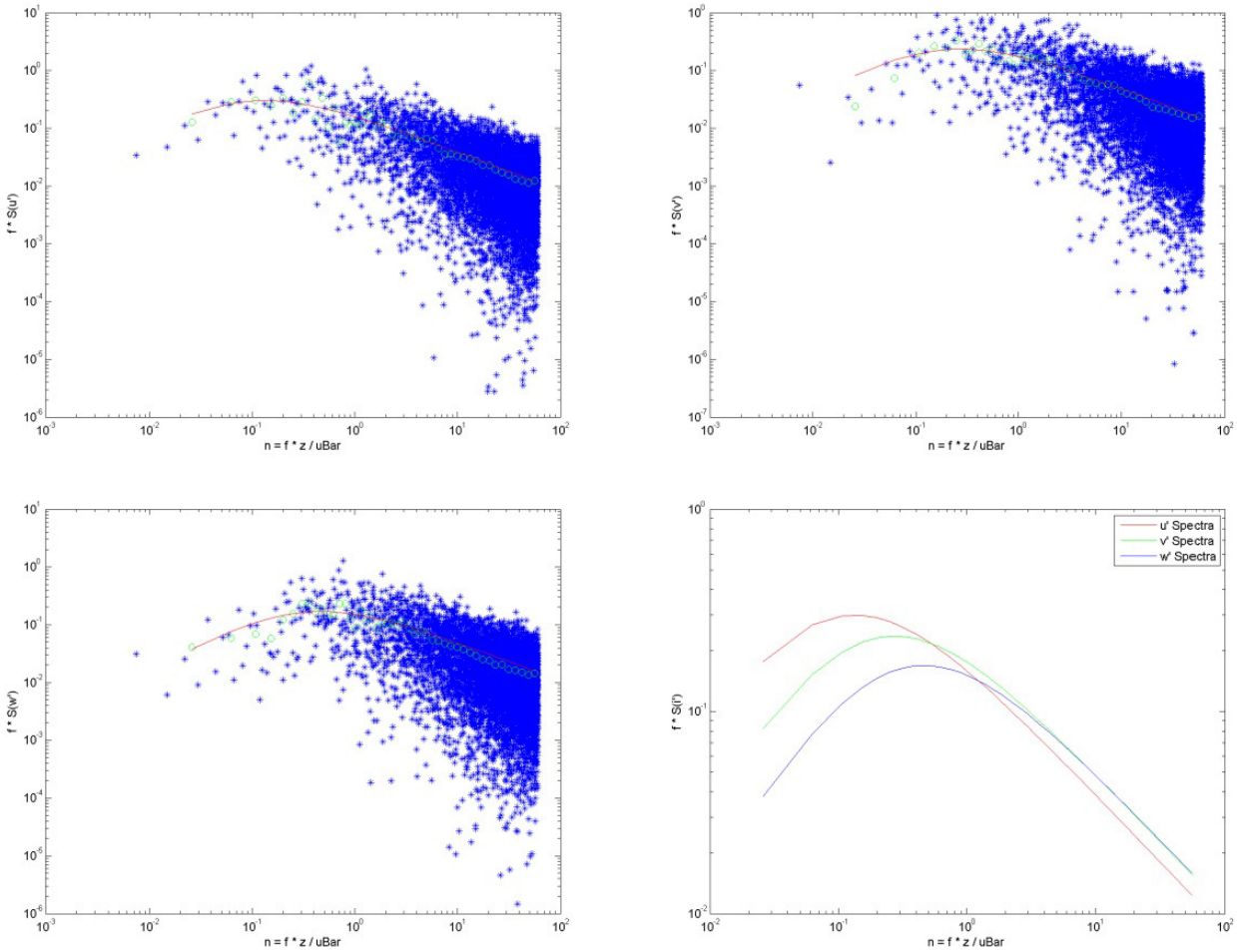

Fig. 2 An example of the turbulence velocity spectra using the curve fitting of (1). Figure 1a is for u, Fig. 1b is for v, and Fig. 1c is for w. The blue dots are from FFT. The green dots result from averages. The red lines represent the fitted u, v, and w spectra of Eq. 1, respectively for a half hour data from level E (42.5 m) on Julian Day 184 (3 July 2003), where $a_u = 26.40$, $b_u = 14.81$ in Fig. 1a, $a_v = 9.839$, $b_v = 7.523$ in Fig. 1b, and $a_w = 2.855$, $b_w = 3.383$ in Fig. 1c. Figure 1d superimposes the fitted spectra for easy comparison.

4. Results

4.1 Urban Canopy Inhomogeneity Effects on Spectral Peaks

As noted in the previous section, the urban canopy of Oklahoma City is highly inhomogeneous. As seen from the building height profile (Fig. 1), the urban canopy is very different for the 4 wind direction sectors. The inhomogeneity of Oklahoma City is also manifested in the difference of the roughness parameter (z_0) and the displacement height (d). We will first examine the effects of this inhomogeneity on the spectral peak frequencies by examining the difference of N_i with respect to the 3 wind direction sectors used in analysis. Table 2 lists the mean peak frequencies, number of runs, standard deviation, and corresponding mean peak wavelength for the 3 WD sectors.

Table 2 Mean spectral peak frequencies, $\overline{N_i}$, *i = u, v, w* at 8 levels with respect to three WD sectors, their number of runs (#), standard deviations (σ_i), and corresponding mean peak wavelengths, $\overline{\Lambda_i}$, *i= u, v, w*

u												
	WD Sector 1(45°–120°)				**WD Sector 2(120°–210°)**				**WD Sector 3(210°–315°)**			
Level	$\overline{N_u}$	$\overline{\Lambda_u(m)}$	σ_u	#	$\overline{N_u}$	$\overline{\Lambda_u(m)}$	σ_u	#	$\overline{N_u}$	$\overline{\Lambda_u(m)}$	σ_u	#
A	0.0430	181.4	0.0156	55	0.0289	269.9	0.0105	843	0.0289	269.9	0.0139	103
B	0.0557	262.1	0.0232	83	0.0461	316.7	0.0170	813	0.0416	351.0	0.0188	140
C	0.0628	342.4	0.0289	105	0.0569	377.9	0.0222	789	0.0498	431.7	0.0236	190
D	0.0684	413.7	0.0355	99	0.0655	432.1	0.0260	805	0.0541	523.1	0.0278	166
E	0.0699	608.0	0.0431	117	0.0824	515.8	0.0350	825	0.0686	619.5	0.0425	138
F	0.0766	728.5	0.0479	102	0.0982	568.2	0.0420	783	0.0777	718.1	0.0442	160
G	0.0924	754.3	0.0548	97	0.1127	618.5	0.0500	810	0.0929	750.3	0.0570	141
H	0.1012	822.1	0.0633	99	0.1223	680.3	0.0561	825	0.1142	728.5	0.0683	163
v												
	WD Sector 1(45°–120°)				**WD Sector 2(120°–210°)**				**WD Sector 3(210°–315°)**			
Level	$\overline{N_v}$	$\overline{\Lambda_v(m)}$	σ_v	#	$\overline{N_v}$	$\overline{\Lambda_v(m)}$	σ_v	#	$\overline{N_v}$	$\overline{\Lambda_v(m)}$	σ_v	#
A	0.0733	106.4	0.0306	56	0.0347	224.8	0.0189	816	0.0354	220.3	0.0236	90
B	0.1312	111.3	0.0552	71	0.071	186.9	0.0398	800	0.0925	157.8	0.0549	127
C	0.1674	128.4	0.0747	100	0.1138	188.9	0.0534	779	0.1248	172.3	0.0709	172
D	0.1623	174.4	0.0873	91	0.1417	199.7	0.0660	803	0.1381	204.9	0.0794	155
E	0.2235	190.2	0.1196	96	0.1958	217.1	0.0904	824	0.1668	254.8	0.1025	127
F	0.2248	248.2	0.1503	95	0.2465	226.4	0.1127	787	0.2144	260.3	0.1310	151
G	0.2601	268.0	0.1727	86	0.2926	238.2	0.1390	807	0.2595	268.0	0.1641	127
H	0.2837	293.3	0.1902	89	0.3282	253.5	0.1563	815	0.2940	283.0	0.1949	142
w												
	WD Sector 1 (45°–120°)				**WD Sector 2(120°–210°)**				**WD Sector 3(210°–315°)**			
Level	$\overline{N_w}$	$\overline{\Lambda_{w(m)}}$	σ_w	#	$\overline{N_w}$	$\overline{\Lambda_w(m)}$	σ_w	#	$\overline{N_w}$	$\overline{\Lambda_{w(m)}}$	σ_w	#
A	0.2440	32.0	0.0375	84	0.1990	39.2	0.0315	846	0.2258	34.5	0.0397	106
B	0.3072	47.5	0.0625	96	0.2300	63.5	0.0425	826	0.2515	58.1	0.0573	148
C	0.3464	62.1	0.0738	102	0.2638	81.5	0.0522	812	0.2888	74.5	0.0790	196
D	0.3677	77.0	0.0984	93	0.2937	96.4	0.0644	837	0.3145	90.0	0.0933	166
E	0.4029	105.5	0.1352	106	0.3347	127.0	0.0847	863	0.3511	121.0	0.1430	141
F	0.3840	145.3	0.1824	104	0.3755	148.6	0.1087	823	0.3762	148.3	0.1737	169
G	0.4258	163.7	0.2265	100	0.4346	160.4	0.1453	855	0.3892	179.1	0.2069	141
H	0.4858	171.3	0.3195	108	0.5074	164.0	0.1849	859	0.4539	183.3	0.2817	173

Based on Table 2, Figs. 3 and 4 show the vertical profiles of the mean non-dimensional peak frequencies ($\overline{N_i}$, $i = u, v, w$) and mean peak wavelengths ($\overline{\Lambda_i}$, $i = u, v, w$) for the 3 WD sectors.

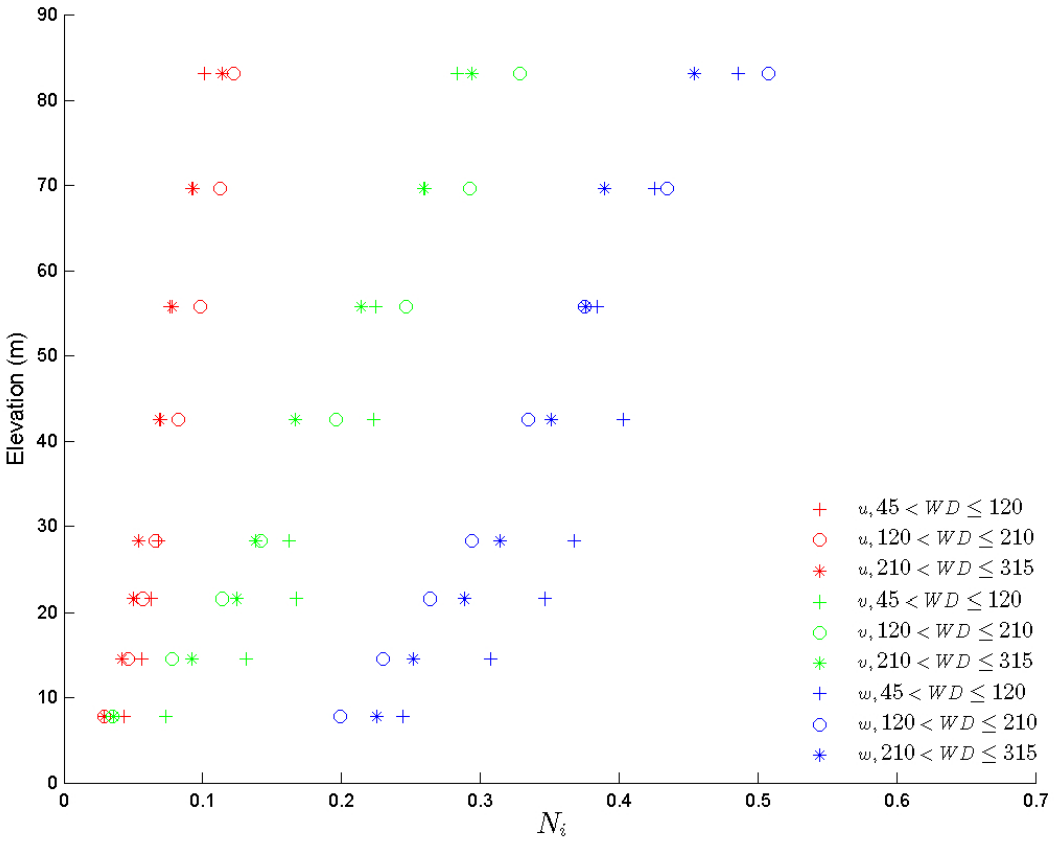

Fig. 3 Vertical profiles of the mean non-dimensional peak frequencies, $\overline{N_i}$, i =u(red), v (green) and w (blue) for the three wind direction sectors: 1) 45°<WD<120°, symbol +; 2) 120° < WD < 210°, symbol o; and 3) 210° < WD < 315°, symbol *

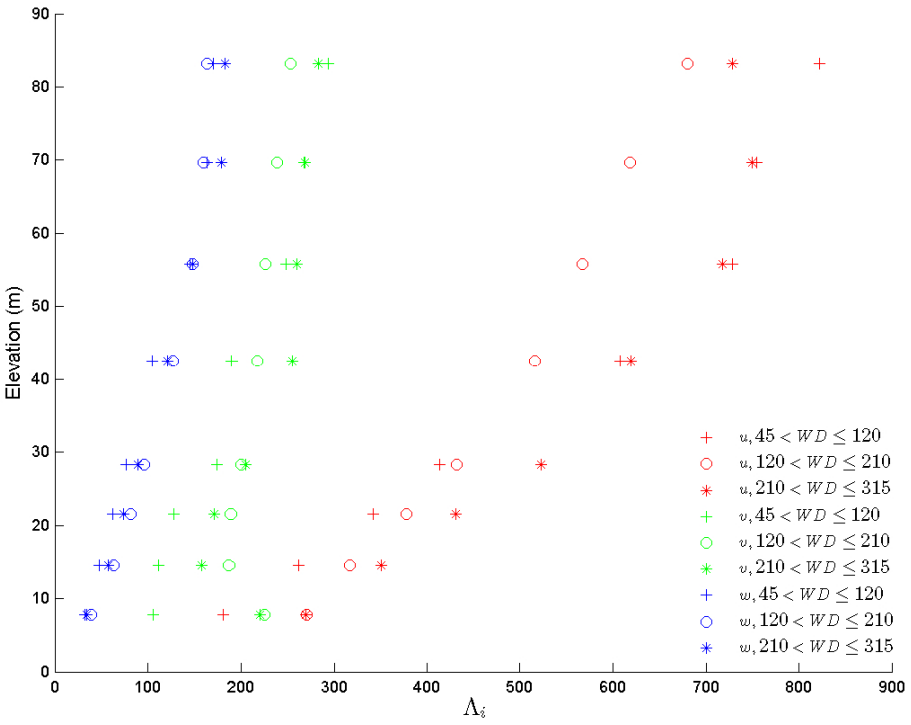

Fig. 4 Same as Fig. 3 except with mean peak wavelengths $\overline{\Lambda_i}$, $i = u,v,w$

The data in Table 2 and on Figs. 3 and 4 show the general features for the mean values of the non-dimensional peak frequency $\overline{N_i}$ and peak wavelengths $\overline{\Lambda_i}$ for the 3 WD sectors as follows:

1. $\overline{N_i}$ increases with height from level A (7.8 m) to level H (83.2 m), as shown in Fig. 3. For example, $\overline{N_u}$ increases from 0.0289 to 0.1233, $\overline{N_v}$ from 0.0347 to 0.3282, and $\overline{N_w}$ from 0.1990 to 0.5074 for WD(2)

2. Likewise, $\overline{\Lambda_i}$ increases with height from level A to level H. $\overline{\Lambda_u}$ increases from 269.9 m to 680.3 m, $\overline{\Lambda_v}$ increases from 224.8 m to 253.5 m, and $\overline{\Lambda_w}$ from 39.2 m to 164.0 m for WD(2).

3. At the same level, there exists

   $\overline{N_u}<\overline{N_v}<\overline{N_w}$
   $\overline{\Lambda_u}>\overline{\Lambda_v}>\overline{\Lambda_w}$

For a further analysis of the impact of the inhomogeneity on the spectral peaks, we can define 3 indices for a certain level as follows

$$\Delta N_i = (\overline{N_i})_{max} - (\overline{N_i})_{min} \tag{9}$$

$$\Delta \Lambda_i = (\overline{\Lambda_i})_{max} - (\overline{\Lambda_i})_{min} \tag{10}$$

$$R_i = \frac{\Delta N_i}{0.5[\ (\overline{N_i})_{max} + (\overline{N_i})\min\ ]} * 100 \tag{11}$$

where the subscripts *max* and *min* indicate the maximum and minimum values of the 3 wind direction sectors at each instrument level. ΔN_i, $\Delta\Lambda_i$, and R_i values are presented in Table 3.

Table 3 Impact on the peak frequencies, ΔN_i, the peak wavelengths, $\Delta\Lambda_i$ and their relative percentage, $R_{i(\%)}$, i = *u, v, w* due to urban canopy inhomogeneity

		u	**v**	**w**
A	ΔN_i	0.0141	0.0386	0.0450
	$\Delta\Lambda_i$	88.5	118.4	7.23
	$R_{i\,(\%)}$	39.2	71.5	20.3
B	ΔN_i	0.0141	0.0531	0.0772
	$\Delta\Lambda_i$	88.9	75.7	16.0
	$R_{i\,(\%)}$	29.0	59.5	28.7
C	ΔN_i	0.130	0.0536	0.0826
	$\Delta\Lambda_i$	89.3	60.5	19.4
	$R_{i\,(\%)}$	23.1	38.1	27.1
D	ΔN_i	0.143	0.0242	0.0740
	$\Delta\Lambda_i$	109.4	30.5	19.4
	$R_{i\,(\%)}$	23.4	32.2	22.4
E	ΔN_i	0.0138	0.0567	0.0682
	$\Delta\Lambda_i$	103.7	64.6	21.5
	$R_{i(\%)}$	18.3	29.1	18.5
F	ΔN_i	0.0216	0.0321	0.0085
	$\Delta\Lambda_i$	160.3	33.9	3.3
	$R_{i\,(\%)}$	24.7	13.9	2.2
G	ΔN_i	0.0203	0.0331	0.0454
	$\Delta\Lambda_i$	135.8	30.4	18.7
	$R_{i\,(\%)}$	19.8	12.0	11.0
H	ΔN_i	0.0211	0.0445	0.0535
	$\Delta\Lambda_i$	141.8	39.8	19.3
	$R_{i\,(\%)}$	18.9	14.5	11.1
Average	ΔN_i	0.0165	0.0420	0.0568
	$\Delta\Lambda_i$	114.7	56.7	15.6
	$R_{i\,(\%)}$	24.5	33.9	17.7

Table 3 implies that the urban canopy inhomogeneity can induce an average of 16–25% variation in spectral peaks both in the mean peak frequencies and mean peak wavelengths. In the lower levels (roughness sublayer), it has the largest impact on N_v, and in the upper levels it has the largest impact on N_u. Its impact on N_w is smaller than that on N_u or N_v. At level A, the impact is very significant. It should also be noted that large changes in N_i and Λ_i in the lowest level occur between WD(1) and WD(3). The difference of mean building height and the roughness length between those 2 WD sectors are only 0.2 m and 0.23 m, respectively. Therefore, it is difficult to

explain the variations in the spectral peaks by either the mean building height or roughness layer changes.

4.2 Atmospheric Stability Effects on the Spectral Peaks

Several parameters can be used to define atmospheric stability for the atmospheric boundary layer (Stull, 1988). Although $\frac{z-d}{L}$ has been used by many authors, we choose to use $\zeta = \frac{z}{L}$ to express the stability where z is the height above the ground, and L is the Obukhov length, since d (the displacement height) is not well-defined for inhomogeneous canopy flow. We have divided the stability ζ into 5 classes:

1. Very unstable $-10.0 < \zeta \leq -0.20$
2. Unstable $-0.20 < \zeta \leq -0.10$
3. Near Neutral $-0.10 < \zeta \leq 0.10$
4. Stable $0.10 < \zeta \leq 0.20$
5. Very Stable $0.20 < \zeta \leq 10.0$

There are very few data points with either $\frac{z}{L}$ smaller than –10.0 or larger than 10.0 that seem unreliable and are, therefore, excluded in our analysis.

Table 4 lists the mean values of the spectral peaks $\overline{N_i}$, $i = u, v, w$ at 8 levels with respect to 5 stability classes, their number of runs (#), standard deviations σ_i, and corresponding mean values of peak wavelengths $\overline{\Lambda_i}$, $i = u, v, w$. The number of runs (#) has a large difference between the 5 stability classes. The near-neutral class has the most data, between 386 and 617 for different levels, and the very stable class has the least data, with no more than 66 samples. In the lower levels there was no very stable case and very few stable cases, which may be related to the urban heat island. The standard deviations appear to increase with height.

Table 4 Mean spectral peak frequencies, $\overline{N}_i$, $i = u, v, w$ at 8 levels with respect to the five stability classes, their number of runs (#), standard deviations (σ_i), and corresponding wavelengths, $\overline{\Lambda}_i$, $i = u, v, w$

Very Unstable (-10.0 < ζ < -0.2)												
	$\overline{N_u}$	#	σ_u	$\overline{\Lambda_u}$	$\overline{N_v}$	#	σ_u	$\overline{\Lambda_v}$	$\overline{N_w}$	#	σ_w	$\overline{\Lambda_w}$
A	0.0217	58	0.0116	359.4	0.017	52	0.0092	458.8	0.2026	63	0.0368	38.5
B	0.0352	56	0.0182	414.8	0.0341	51	0.0246	428.2	0.227	63	0.0544	64.32
C	0.0446	77	0.0212	482.1	0.0495	64	0.0275	434.3	0.2346	80	0.0514	91.65
D	0.0466	101	0.0235	607.3	0.0668	85	0.0401	423.7	0.2472	107	0.0597	114.5
E	0.0549	152	0.0271	774.1	0.0985	131	0.0667	431.5	0.2647	161	0.0736	160.6
F	0.0683	151	0.037	817	0.1185	137	0.0729	470.9	0.2756	168	0.0778	202.5
G	0.0777	173	0.0409	897	0.135	158	0.0786	516.3	0.3012	196	0.1014	231.4
H	0.0832	199	0.0489	1000	0.1513	184	0.079	549.9	0.3335	219	0.1194	249.5
Unstable (-0.2< ζ < -0.1)												
	$\overline{N_u}$	#	σ_u	$\overline{\Lambda_u}$	$\overline{N_v}$	#	σ_u	$\overline{\Lambda_v}$	$\overline{N_w}$	#	σ_w	$\overline{\Lambda_w}$
A	0.0256	166	0.0102	304.7	0.0222	157	0.0131	351.4	0.195	167	0.029	40
B	0.0401	158	0.0146	364.1	0.0455	148	0.0266	320.9	0.2157	157	0.0373	67.69
C	0.0497	163	0.0212	432.6	0.0768	155	0.0438	279.9	0.2498	166	0.049	86.07
D	0.0548	166	0.024	516.4	0.0921	166	0.0481	307.3	0.2685	170	0.0583	105.4
E	0.0684	187	0.0272	621.3	0.137	187	0.0658	310.2	0.3005	191	0.0589	141.4
F	0.08	172	0.0349	697.5	0.1786	167	0.0739	312.4	0.3269	174	0.071	170.7
G	0.0869	167	0.0387	802.1	0.2106	165	0.0783	331	0.3689	169	0.0789	188.9
H	0.0866	148	0.0382	960.7	0.2393	152	0.084	347.7	0.424	153	0.093	196.2
Near-Neutral (-0.1< ζ < 0.1)												
	$\overline{N_u}$	#	σ_u	$\overline{\Lambda_u}$	$\overline{N_v}$	#	σ_u	$\overline{\Lambda_v}$	$\overline{N_w}$	#	σ_w	$\overline{\Lambda_w}$
A	0.0304	617	0.0100	256.6	0.0394	605	0.0184	198.0	0.1996	614	0.0312	39.08
B	0.0486	598	0.0166	300.4	0.0899	600	0.0363	162.4	0.2339	605	0.0416	62.42
C	0.0607	548	0.0214	354.2	0.1311	558	0.0467	164.0	0.2714	563	0.0503	79.22
D	0.0722	535	0.024	392.0	0.1672	546	0.0548	169.3	0.3086	554	0.0585	91.70
E	0.0951	469	0.032	464.9	0.2387	480	0.0657	178	0.3633	486	0.0710	117.0
F	0.1114	414	0.0357	500.9	0.2998	435	0.0831	186.1	0.4147	434	0.0866	134.6
G	0.1289	402	0.0421	540.7	0.3584	415	0.1026	194.5	0.4812	420	0.1042	144.8
H	0.1425	386	0.0436	583.9	0.4037	387	0.1034	206.1	0.5712	389	0.1268	145.7

Table 4 Mean spectral peak frequencies, $\overline{N_i}$, $i = u, v, w$ at 8 levels with respect to the five stability classes, their number of runs (#), standard deviations (σ_i), and corresponding wavelengths, $\overline{\Lambda_i}$, $i = u, v, w$ (continued)

Stable (0.1< ζ < 0.2)												
	$\overline{N_u}$	#	σ_u	$\overline{\Lambda_u}$	$\overline{N_v}$	#	σ_u	$\overline{\Lambda_v}$	$\overline{N_w}$	#	σ_w	$\overline{\Lambda_w}$
A	0.0408	2	0.0057	191.2	0.0482	2	0.0292	161.8	0.2127	2	0.1221	36.67
B	0.0674	1	0	216.6	0.1126	1	0	129.7	0.2884	1	0	50.62
C	0.0914	1	0	235.2	0.2284	1	0	94.1	0.3702	2	0.0292	58.08
D	0.1043	3	0.0278	271.3	0.27	5	0.0592	104.8	0.4456	5	0.0390	63.51
E	0.1368	11	0.025	310.7	0.2993	16	0.0605	142	0.4803	16	0.0976	88.49
F	0.1473	25	0.0383	378.8	0.3706	26	0.0877	150.6	0.5411	26	0.0828	103.1
G	0.1611	27	0.0436	432.7	0.4582	29	0.0898	152.1	0.6763	29	0.0982	103.1
H	0.1731	32	0.0392	480.6	0.546	31	0.0939	152.4	0.7468	32	0.1276	111.4
Very Stable (0.2< ζ <10.0)												
	$\overline{N_u}$	#	σ_u	$\overline{\Lambda_u}$	$\overline{N_v}$	#	σ_u	$\overline{\Lambda_v}$	$\overline{N_w}$	#	σ_w	$\overline{\Lambda_w}$
A	0	0	0		0	0	0		0	0	0	
B	0	0	0		0	0	0		0	0	0	
C	0	0	0		0.1825	1	0	117.8	0.4298	1	0	50.02
D	0	0	0		0.1849	1	0	153.1	0.4949	1	0	57.18
E	0.1201	6	0.0359	353.8	0.3476	10	0.0755	122.3	0.5163	9	0.0473	82.32
F	0.1449	21	0.0407	385.1	0.3568	22	0.1084	156.4	0.5633	21	0.1011	99.06
G	0.1749	41	0.0435	398.5	0.4494	40	0.1010	155.1	0.6954	41	0.1181	100.2
H	0.1838	60	0.0590	452.7	0.4939	61	0.1287	168.5	0.7860	66	0.1723	105.9

Based on Table 4, Figs. 5 and 6 show the vertical profiles of the mean non-dimensional peak frequencies $\overline{N_i}$ and mean peak wavelengths $\overline{\Lambda_i}$ for the 5 stability classes.

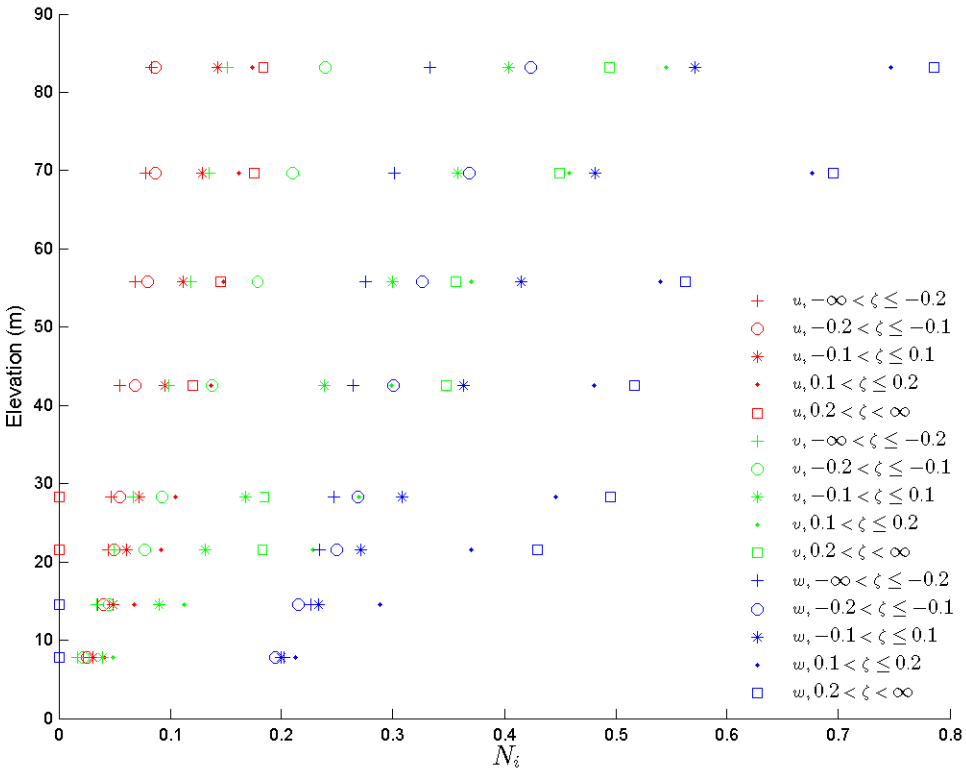

Fig. 5 Vertical profiles of the mean non-dimensional peak frequencies, $\overline{N_i}$, $i = u$ (red), v (green) and w (blue) for wind direction (WD) sector 2, with respect to the 5 stability categories

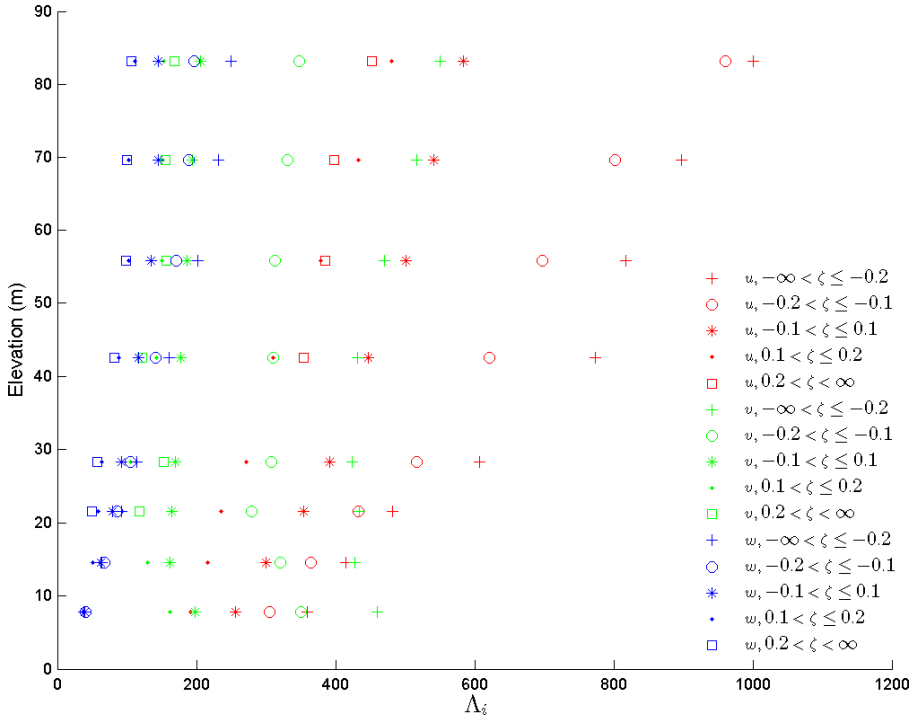

Fig. 6 Same as Fig. 5 except for the mean peak wavelengths, Λ_i, $i = u, v, w$

Table 4 and Figs. 5 and 6 show the following features for the mean value of the non-dimensional peak frequencies $\overline{N_i}$ and mean peak wavelengths $\overline{\Lambda_i}$.

1. The values of spectral peaks $\overline{N_i}$, $i = u, v, w$ increase with increasing stability at a fixed level. For example, $\overline{N_w}$ at level H increases from 0.334 for very unstable conditions to 0.786 for the very stable category. Likewise, the mean values of peak wavelength at a fixed level decrease with stability (Table 4). For instance, the mean peak wavelength of *w* at level H decreases from 249.5 m to 105.9 m.

2. Both $\overline{N_i}$ and $\overline{\Lambda_i}$ increase with height, as evidenced in Figs. 5 and 6. For instance, $\overline{N_w}$ increases from 0.203 at level A to 0.334 at level H, while $\overline{\Lambda_w}$ goes from 38.5 m to 249.5 m (Table 4).

In order to quantify the impact of the atmospheric stability on the spectral peaks, we have calculated the values of ΔN_i, $\Delta \Lambda_i$, and R_i, as defined by Eqs. 9, 10, and 11 from Table 4, where the subscripts *max* and *min* indicate the maximum and minimum of the 5 stability categories at each instrument height. These values are listed in Table 5.

Table 5 Impact on the peak frequencies, ΔN_i, the peak wavelengths, $\Delta\Lambda_i$ and their relative percentage, $R_{i\,(\%)}$, $i = u, v, w$ due to atmospheric stability

		u	**v**	**w**
A	ΔN_i	0.0191	0.0312	0.0177
	$\Delta\Lambda_i$	168.2	297.0	3.33
	$R_{i\,(\%)}$	61.1	95.7	8.7
B	ΔN_i	0.0322	0.0785	0.0727
	$\Delta\Lambda_i$	198.2	298.5	17.1
	$R_{i(\%)}$	62.8	107.0	28.8
C	ΔN_i	0.0468	0.1789	0.1952
	$\Delta\Lambda_i$	246.9	340.2	41.6
	$R_{i(\%)}$	68.8	128.8	58.8
D	ΔN_i	0.0577	0.2032	0.2477
	$\Delta\Lambda_i$	336.0	318.9	57.32
	$R_{i\,(\%)}$	76.5	120.7	66.8
E	ΔN_i	0.0819	0.2491	0.2516
	$\Delta\Lambda_i$	463.4	309.2	78.3
	$R_{i\,(\%)}$	85.5	111.7	64.5
F	ΔN_i	0.0790	0.2521	0.2877
	$\Delta\Lambda_i$	438.2	320.3	103.4
	$R_{i\,(\%)}$	73.3	103.1	68.6
G	ΔN_i	0.0972	0.3232	0.3942
	$\Delta\Lambda_i$	498.5	364.2	131.2
	$R_{i\,(\%)}$	77.0	109.0	79.1
H	ΔN_i	0.1006	0.3947	0.4525
	$\Delta\Lambda_i$	547.3	397.5	143.6
	$R_{i\,(\%)}$	75.4	113.2	80.8
Average	ΔN_i	0.0643	0.2139	0.2399
	$\Delta\Lambda_i$	362.1	330.7	71.98
	$R_{i\,(\%)}$	72.5	111.1	57.0

Table 5 indicates that the atmospheric stability can cause an average of 43–71% variation in spectral peaks, both in the mean peak frequencies and mean peak wavelengths. It has the largest effects on the *v* spectra. The stability impacts on the mean spectral peaks have more or less the same degree for the different levels, except for the lowest level *w* spectra, with only 8% change on average. This shows that atmospheric stability impacts are stronger and more significant than urban canopy inhomogeneity, indicated by comparing Table 5 with Table 3, particularly for upper levels.

To further investigate the relationship between the non-dimensional peak frequency N_i and the atmospheric stability, we have used an exponential expression which is

$$N_i = a\ |\zeta|^b + c \tag{12}$$

where *a, b,* and *c* are constants determined by observed data. The data from 3 levels (levels E, F, and G) have been lumped together for the curve fitting of Eq. 12, with results presented in Fig. 7. To fit Eq. 12, 30 bin averages of N_i and *z/L* have been used, 15 to fit the positive data and 15 to fit the negative *z/L* data. Figure 7 shows a representative relationship between N_i and *z/L* in a layer (42.5–69.7 m) above the Oklahoma urban canopy, with a displacement height of 19.9 m in the wind direction range of 120–210°. These results are similar to those over flat land (Figure 2.9, Kaimal and Finnigan 1994).

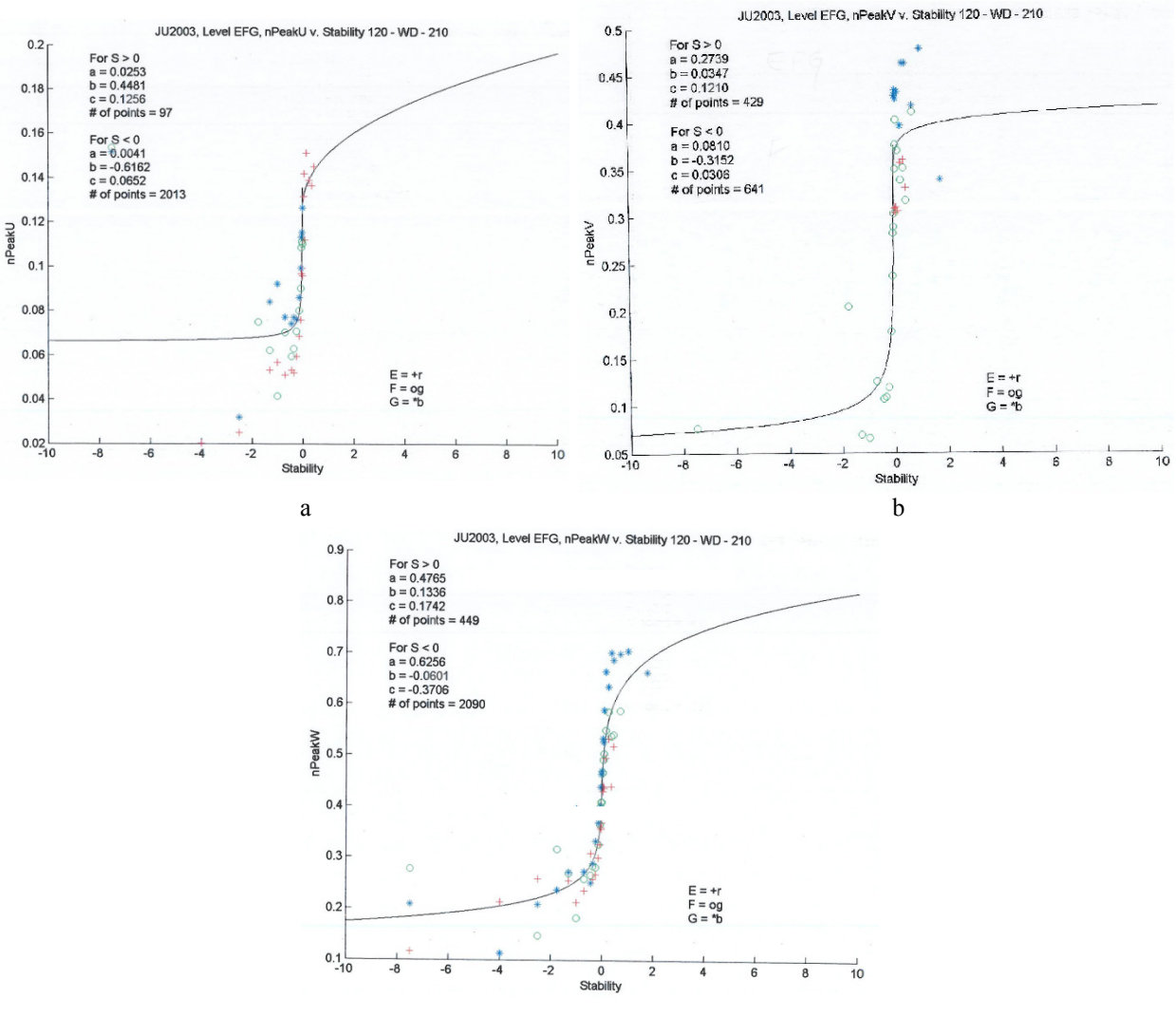

Fig. 7 Variation of the spectral peaks with the stability (*z/L*) for $\overline{N}_u$ (Fig. 7a), $\overline{N}_v$ (Fig. 7b), and $\overline{N}_w$ (Fig. 7c) composed from 3 levels (level E,F,G) for 120°<WD<210°. The curves in the Fig. 7 are from the empirical curve fitting, Eq. 12.

4.3 Observational Height (z) Effects on the Spectral Peaks

Figures 3, 4, 5, and 6 have clearly shown the effects of observational height (z) on the spectral peaks. We mentioned earlier that both the mean non-dimensional peak frequencies and the peak wavelengths increase with z for all 3 WD sectors (Table 2) and for all 5 atmospheric stability classes (Table 4). Here we can compare the relative importance of the 3 factors by using the index R_i, defined in (10).

The 8 level averaged R_i values for the 3 factors (WD, stability, and z) are listed in Table 6.

Table 6 Comparison of relative effects of the wind direction (WD), atmospheric stability (z/L), and observational height (z) on the u-, v-, and w-spectral peaks

	U spectra	**V spectra**	**W spectra**
WD	24.5 %	33.9 %	17.7 %
z/L	72.5 %	111.1 %	57.0 %
z	120.7 %	166.0 %	93.9 %

The averaged values of R_i in the first 2 lines of Table 6 are from the last lines of Tables 2 and 4, respectively. The averaged values of R_i in the third line of Table 6 are based on Table 4 for the stable, near-neutral, and unstable stratification. From the numbers listed above, it is clear that the observation height plays a dominant role for spectral peaks. For example, the change of z from 7.8 m to 83.2 m can affect the average peak value of w-spectra by 93.9%, while the change in the stability (z/L) from very stable to very unstable stratification, or the change in the wind direction can cause the average peak values by 57.0% and 17.7%, respectively.

The spectral fit parameters, a_i and b_i, also change with z significantly. Figure 8 exhibits the average spectral fits of the u, v, and w spectra at 8 levels (A through H) for the near-neutral conditions. Notice that the average u, v, and w spectra at different levels are plotted with different colors. The figures cover $120° < WD < 210°$. Related to Fig. 8 is Table 7, which provides the mean near-neutral spectra parameters, $\overline{a_i}$ and $\overline{b_i}$ in (1), $i = u, v, w$, their standard deviations (σ_a, σ_b), number of runs (#), corresponding mean peak frequencies $\overline{N_i}$ and mean peak wavelengths $\overline{\Lambda_i}$.

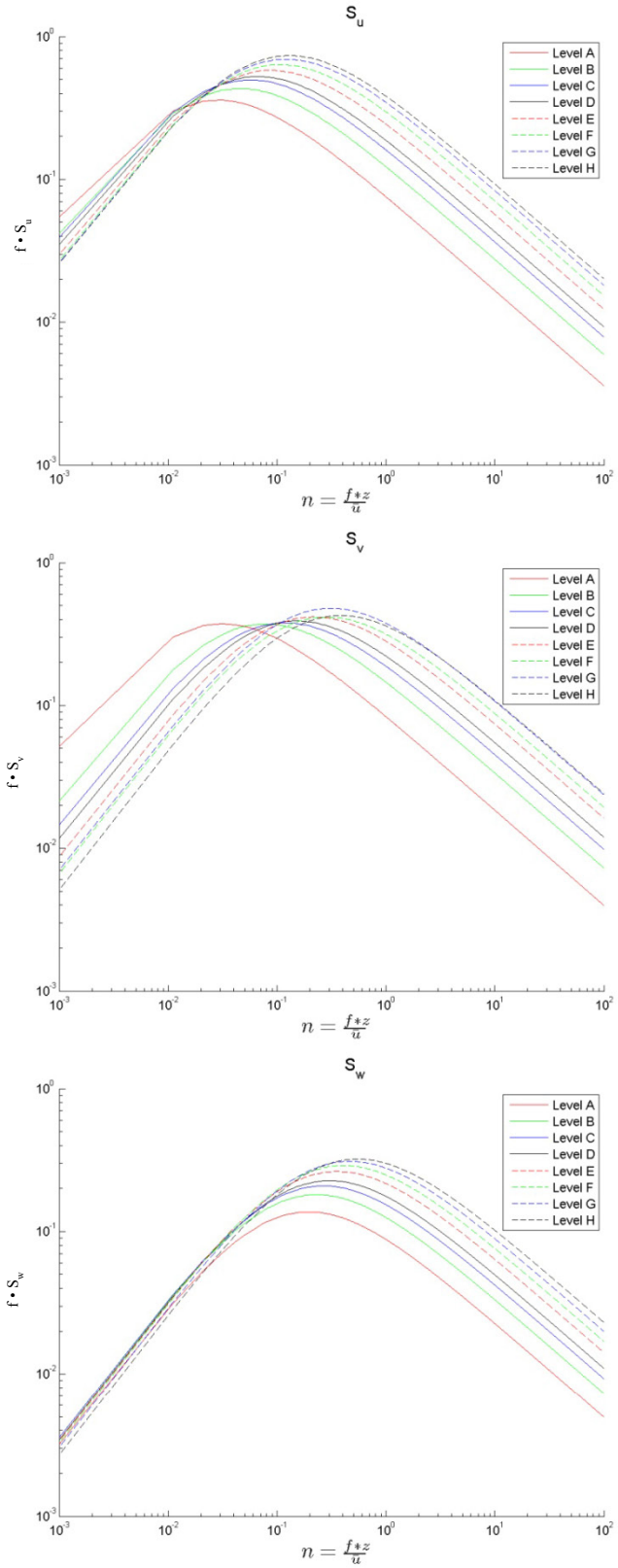

Fig. 8 The average spectra of *u*, *v*, and *w* at eight levels for the near-neutral conditions

Figure 8 clearly shows the systematic variation of these spectral parameters with height above the ground. All of the peaks of *u*, *v*, and *w* spectra move toward high frequency from lower levels to higher levels. Table 7 shows that those mean peak frequencies and mean peak wavelengths increase with height. For example, the non-dimensional peak frequency of near-neutral *w* spectra increases from 0.194 at 7.8 m to 0.544 at 83.2 m. The corresponding average peak wavelengths increase from 40.2 m at 7.8 m to 152.9 m at 83.2 m.

Table 7 Mean near-neutral spectral parameters, $\overline{a_i}$ and $\overline{b_i}$ in (1), $i = u, v, w$, their standard deviations (σ_a and σ_b), number of runs (#), corresponding mean peak frequencies $\overline{N_i}$, and mean peak wavelengths $\overline{\Lambda_i}$

u							
Level	$\overline{a_i}$	$\overline{b_i}$	σ_a	σ_b	#	$\overline{N_i}$	$\overline{\Lambda_i}$
A	59.503	53.8397	40.8961	18.8265	805	0.0279	280.0
B	44.2428	33.3098	31.9081	12.2455	761	0.045	324.2
C	41.1913	26.9471	33.1569	11.0933	669	0.0557	386.2
D	36.5341	22.7017	29.6500	10.6749	652	0.0661	428.3
E	30.7313	17.263	27.8519	7.9642	595	0.0869	489.1
F	27.9296	14.3053	23.4567	5.7995	552	0.1049	532.1
G	26.8645	12.6385	23.8325	5.3274	531	0.1187	587.2
H	26.4446	11.7285	27.6094	5.5186	476	0.1279	650.6
v							
Level	$\overline{a_i}$	$\overline{b_i}$	σ_a	σ_b	#	$\overline{N_i}$	$\overline{\Lambda_i}$
A	56.0646	48.8256	115.1372	49.491	805	0.0307	253.9
B	22.240	19.5067	31.0581	14.3552	761	0.0769	189.9
C	14.857	12.7861	16.0955	6.6412	669	0.1173	183.3
D	11.928	9.9605	13.2049	5.4454	652	0.1506	187.9
E	8.8595	6.9298	23.2993	7.7251	595	0.2165	196.3
F	6.7696	5.3005	4.2196	1.7542	552	0.2830	197.2
G	7.1111	4.842	25.3765	7.2713	531	0.3098	225.0
H	5.1598	3.9461	2.8262	1.1992	476	0.3801	218.9
w							
Level	$\overline{a_i}$	$\overline{b_i}$	σ_a	σ_b	#	$\overline{N_i}$	$\overline{\Lambda_i}$
A	3.2521	7.7382	1.6606	1.3018	805	0.1938	40.24
B	3.6413	6.5633	1.8548	1.1597	761	0.2285	63.88
C	3.6213	5.6603	1.8499	1.0342	669	0.2650	81.13
D	3.4702	4.9885	1.8359	0.9646	652	0.3007	94.12
E	3.4229	4.2448	1.8160	0.8555	595	0.3534	120.3
F	3.3235	3.7405	1.6930	0.8028	552	0.4010	139.2
G	3.0773	3.2389	1.4198	0.6842	531	0.4631	150.5
H	2.7193	2.7570	1.1437	0.6147	476	0.5441	152.9

5. Conclusion

Previous methods for determining the spectral peaks have their limitations. The direct outputs from FFT are very noisy, which cannot provide accurate estimates for spectral peaks. The bin average method has limited resolution and, therefore, limited accuracy for evaluation of spectral peaks. Our simple analytical form to model one-dimensional velocity spectra appears very useful and dependable. Different analytical expressions (Sorbjan, 1989), of course, can be used to model velocity spectra, but they are not necessarily better than the simple one, such as Eq. 1. Based on this simple analytical expression, the one-dimensional velocity spectral characteristics from the Oklahoma City (JU2003) sonic measurements have been analyzed extensively.

In the tower layer (7.8–83.2 m) at Oklahoma City downtown, the mean values of dimensionless spectral peaks can vary widely—0.022–0.184 for *u* spectra, 0.017–0.546 for *v*, and 0.203–0.786 for *w*. The corresponding mean peak wavelengths can be 191–1000 m for *u* spectra, 94–550 m for *v,* and 37–250 m for *w*, depending on wind direction, atmospheric stability (*z/L*), and the observation height (*z*). There are 3 factors, at least, that have significant impacts on these mean spectral peaks. 1) The wind direction factor which takes the complex influences of the building distribution along the fetch. 2) The atmospheric stability (*z/L*) factor which causes $\overline{N_i}$ increases with the stability (larger *z/L* value) and $\overline{\Lambda_i}$ decreases with stability, $i = u, v,$ and *w*, as evidenced in Table 4. This factor seems more pronounced than the first factor. 3) The observation height (*z*) factor, which is a more pronounced influence than either the stability or wind direction.

It is very interesting that the spectral peak locations under near neutral conditions vary with height systematically, as shown in Fig. 8. It should be pointed out that the classic Monin-Obukhov parameter (*z/L*) appears to be not the only factor in determining those spectral peaks for the inhomogeneous urban canopy flow, such as in the Oklahoma City case. It is still a large challenge to formulate a theoretical similarity formulation, if any, for this complex canopy flow.

6. References

Allwine KJ, Leach MJ, Stockham LW, Shinn JS, Hosker RP, Bowers JF, Pace JC. Overview of joint urban 2003 – an atmospheric dispersion study in Oklahoma City. AMS Symposium on Planning, Nowcasting, and Forecasting in the Urban Zone, 11–15 January 2004, Seattle, WA, 2004.

Busch NE, Panofsky HA. Recent spectra of atmospheric turbulence. Q J R Meteorol. Soc. 1968;94:132–148.

Chang SS, Huynh GD, Klipp CL, Williamson CC, Garvey DM, Wang Y. Observational study of turbulence spectra for joint urban 2003. Amer. Meteor. Soc. 5th Symposium on Urban Environment, 23–27 Aug., Vancouver, BC, Canada, 3.5, 2004.

Chang Sam, Huynh Giap. A comparison of roughness parameters for Oklahoma City from different evaluation methods. Seventh Symposium on the Urban Environment, 10–13 September, 2007, San Diego, CA, American Meteorological Society.

Chang S, Huynh G, Tofsted D. Turbulence characteristics in Oklahoma City measured from a 83 m pseudo tower. The 89th AMS Annual Meeting, 11–15 January 2009, Phoenix, Arizona, USA.

Chang Sam, Huynh G, Tofsted D, Garvey D, Williamson C, Li D. Urban turbulence spectra from field observation. The 16th Conference on Air Pollution Meteorology, 2010 AMS Annual Meeting, 17–21 January 2010, Atlanta, Georgia USA.

Feigenwinter C, Vogt R, Parlow E. Vertical structure of turbulence above an urban canyon, pp 472–473 in Preprints of the 12th symposium of boundary layer and turbulence. Vancouver, Canada, July 28–August 1, 1997, American Meteorological Society, Boston, USA.

Feigenwinter C, Vogt R, Parlow E. Vertical structure of selected turbulence characteristics above an urban canopy. Theoretical and Applied Climatology. 1999;62:51–63.

Gouveia FJ, Leach MJ, Shinn JM, Ralph WE. Use of a large crane for wind and tracer profiles in an urban setting. Journal of Atmospheric and Oceanic Technology. 2007;24:1750–1756.

Kaimal JC, Finnigan JJ. Atmospheric Boundary Layer Flows, Their Structure and Measurement. Oxford University Press, 1994, 289 pp.

Lee X, Massman W, Law B. Handbook of micrometeorology, 2004, pp 250.

Lundquist JK, Shinn JH, Gouveia F. Observations of turbulent kinetic energy dissipation rate in the urban environment. 84th AMS Annual Meeting, 11–15 January 2004, Seattle, WA, 2004.

Panofsky Hans A. Dutton John A. Atmospheric turbulence. John Wiley & Sons, 1984, 397 pp.

Roth M. Review of atmospheric turbulence over Cities. Q J R. Meteorol. Soc. 2000;126:941–990.

Sorbja, Z. Structure of the atmospheric boundary layer. Prentice-Hall, Inc., 1989, 317 pp.

Wilson D Keith. A new model for turbulence spectra and correlations based on meijer's G-functions. Adelphi (MD): US Army Research Laboratory (US). February 1998. Report No.: ARL-TN-104.

1 (PDF) DEFENSE TECHNICAL INFORMATION CTR DTIC OCA

2 (PDFS) DIRECTOR US ARMY RESEARCH LAB RDRL CIO LL IMAL HRA MAIL & RECORDS MGMT

1 (PDF) GOVT PRINTG OFC A MALHOTRA

14 (HCS) US ARMY RESEARCH LAB RDRL CIE D

2 (PDFS) S CHANG (4 HCS, 1 PDF)
C KLIPP (1 HC)
G HUYNH (1 HC)
Y WANG (1 HC)
P CLARK (1 HC)
S O'BRIEN (4 HCS, 1 PDF)
G VAUCHER (1 HC)
R RANDALL (1 HC)

INTENTIONALLY LEFT BLANK.